Wiley Online Library
Early View publication on www.wileyonlinelibrary.com
(issue and page numbers not yet assigned;
citable using Digital Object Identifier – **DOI**)

Phys. Status Solidi A, 1–7 (2016) / **DOI** 10.1002/pssa.201532855

physica status solidi a
www.pss-a.com
applications and materials science

Valence-band electronic structure evolution of graphene oxide upon thermal annealing for optoelectronics

Hisato Yamaguchi[*,1], Shuichi Ogawa[2], Daiki Watanabe[2], Hideaki Hozumi[2], Yongqian Gao[†,3], Goki Eda[4,5,6], Cecilia Mattevi[7], Takeshi Fujita[8], Akitaka Yoshigoe[9], Shinji Ishizuka[10], Lyudmyla Adamska[11,12], Takatoshi Yamada[13], Andrew M. Dattelbaum[1], Gautam Gupta[1], Stephen K. Doorn[3], Kirill A. Velizhanin[11], Yuden Teraoka[9], Mingwei Chen[8], Han Htoon[3], Manish Chhowalla[14], Aditya D. Mohite[,1], and Yuji Takakuwa[***,2]**

[1] MPA-11 Materials Synthesis and Integrated Devices (MSID), Materials Physics and Applications (MPA) Division, Mail Stop: K763, Los Alamos National Laboratory (LANL), P.O. Box 1663, Los Alamos, New Mexico 87545, USA
[2] Institute of Multidisciplinary Research for Advanced Materials (IMRAM), Tohoku University, 2-1-1 Katahira, Aoba-ku, Sendai 980-8577, Japan
[3] Center for Integrated Nanotechnologies (CINT), MPA Division, Mail Stop: K771, LANL, P.O. Box 1663, Los Alamos, New Mexico 87545, USA
[4] Department of Physics, National University of Singapore, 2 Science Drive 3, Singapore 117542
[5] Department of Chemistry, National University of Singapore, 3 Science Drive 3, Singapore 117543
[6] Graphene Research Centre, National University of Singapore, 6 Science Drive 2, Singapore 117546
[7] Department of Materials, Imperial College London, Exhibition Road, London SW7 2AZ, UK
[8] WPI Advanced Institute for Materials Research (AIMR), Tohoku University, 2-1-1 Katahira, Aoba-ku, Sendai, Miyagi 980-8577, Japan
[9] Quantum Beam Science Directorate, Japan Atomic Energy Agency, Kouto, Sayo-cho, Sayo-gun, Hyogo 679-5198, Japan
[10] Department of Materials Science and Engineering, Akita National College of Technology, 1-1 Bunkyo-machi, Iigima, Akita 011-8511, Japan
[11] T-1 Physics and Chemistry of Materials, Theoretical Division, Mail Stop: B221, LANL, P.O. Box 1663, Los Alamos, New Mexico 87545, USA
[12] Center for Nonlinear Studies (CNLS), Theoretical Division, Mail Stop: B258, LANL, P.O. Box 1663, Los Alamos, New Mexico 87545, USA
[13] Nanotube Research Center, National Institute of Advanced Industrial Science and Technology (AIST), 1-1-1 Umezono, Tsukuba, Ibaraki 305-8568, Japan
[14] Department of Materials Science and Engineering, Rutgers University, 607 Taylor Road Piscataway, New Jersey 08854, USA

Received 20 October 2015, revised 1 March 2016, accepted 18 March 2016
Published online 8 April 2016

Keywords Fermi level, graphene oxide, optoelectronic, ultraviolet photoelectron spectroscopy, valence-band electronic structure

[*] Corresponding author: e-mail hyamaguchi@lanl.gov, Phone: +1 505 664 0382, Fax: +1 505 667 9905
[**] e-mail amohite@lanl.gov, Phone: +1 505 665 2246, Fax: +1 505 667 9905
[***] e-mail takakuwa@tagen.tohoku.ac.jp, Phone: +81 22 217 5365, Fax: +81 22 217 5405
[†]Present address: Key Laboratory of Flexible Electronics (KLOFE) and Institute of Advanced Materials (IAM), Jiangsu National Synergetic Innovation Center for Advanced Materials (SICAM), Nanjing Tech University (NanjingTech), 30 South Puzhu Road, Nanjing 211816, P. R. China.

We report valence-band electronic structure evolution of graphene oxide (GO) upon its thermal reduction. The degree of oxygen functionalization was controlled by annealing temperature, and an electronic structure evolution was monitored using real-time ultraviolet photoelectron spectroscopy. We observed a drastic increase in the density of states around the Fermi level upon thermal annealing at ~600 °C. The result indicates that while there is an apparent bandgap for GO prior to a thermal reduction, the gap closes after an annealing around that temperature. This trend of bandgap closure was correlated with the electrical, chemical, and structural properties to determine a set of GO material properties that is optimal for optoelectronics. The results revealed that annealing at a temperature of ~500 °C leads to the desired properties, demonstrated by a uniform and an order of magnitude enhanced photocurrent map of an individual GO sheet compared to an as-synthesized counterpart.

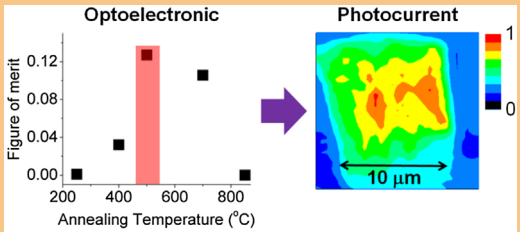

1 Introduction Graphene has extraordinary physical properties, making it potentially useful as a material for next-generation electronic and optoelectronic devices [1, 2]. It is a semimetal with an extraordinary high charge carrier mobility of 200 000 $cm^2/V\,s$, and possesses a high optical transmittance of 98.7% in the visible range due to the material's atomically thin nature, yet it is mechanically stable [3–5]. The fundamental bottleneck of its pristine form, however, is a lack of intrinsic bandgap. Stacking multiple layers of graphene induces a bandgap but it is in the range of a few tens to a hundred meV [6] thus too small for many of applications. Nanoribbons of graphene with a width range of a few tens of nm will also exhibit bandgaps (few hundred meV) but their fabrication process generally requires sophisticated instrumentations, and the gap is very sensitive to the width and edge states [7, 8]. Recently, a number of reports have demonstrated the potential of chemical functionalization as a promising alternative route to gain tunability in graphene electronic structure. More specifically, fluorination and hydrogenation of graphene open up a bandgap that is as large as one to a few eV [9–12]. While these chemical functionalization hold promise toward the tunability of graphene electronic structure for practical devices, the functionalization processes generally require vacuum-based system and elevated temperatures (400–600 °C) [9, 10] with an exception of recent efforts using a laser-assisted photochemical method [13, 14]. These process requirements can be disadvantageous for applications such as flexible and organic electronics/optoelectronics, for which the low-temperature and low-cost processing are crucial.

Functionalization using oxygen is an attractive candidate for this purpose. While an atomically controlled functionalization using oxygen gas remains challenging [15], inhomogeneous but relatively high oxidization of graphene up to 40 at.% is readily possible via simple chemical oxidization of graphite powders at room temperature (referred to as graphene oxide (GO)) [16–18]. In addition, the material properties can be tuned by removing oxygen at nearly room temperature via a chemical route [16, 17, 19–23]. Further chemical reduction is possible via e-beam [24] and laser irradiation [25]. It is well-established from the electrical characterization that a chemical reduction process can restore the semi-metallic property of GO from an insulator [17, 26–29].

In this study, we performed real-time ultraviolet photoelectron spectroscopy (UPS) of as-synthesized GO upon thermal reduction. A detailed valence-band (VB) electronic structure evolution with emphasis on the density of states (DOS) for carbon 2p π bonds and the Fermi level E_F were monitored up to 850 in 50 °C steps. As a result, a sharp increase of DOS around the E_F was observed at annealing temperatures between 600 and 650 °C indicating a bandgap closure [30]. A comparison between the VB electronic structure evolutions and electrical conductivity suggested that an annealing temperature of ~500 °C would lead to material properties suitable for GO-based optoelectronics. This was demonstrated by a photocurrent map, which an individual GO sheet reduced at ~500 °C exhibited a uniform and an order of magnitude enhanced photocurrent over an entire sheet compared to an as-synthesized counterpart. Our results pave a pathway for a design of optimized graphene-based optoelectronic devices by providing the key values that are related to the electronic structures of GO having different densities of chemical functional groups.

2 Experimental

2.1 Synthesis of GO, thin-film deposition, and individual sheet device fabrication GO was prepared via a modified Hummer's method [31]. Briefly, graphite powders (Asbury Carbon Inc.) with an average flake size of ~500 μm were chemically oxidized for 5 days at room temperature in a mixture of sulfuric acid, sodium nitrate, and potassium permanganate at a chemical equilibrium state and exfoliated. After removal of residual metal ions and unexfoliated graphitic particles by continuous washing using deionized (DI) water and repeated centrifugation, respectively, a dilute GO suspension in DI water was prepared for thin-film deposition. GO films with thickness of ~5 nm were deposited using vacuum filtration on cellulose membrane supports [17], which were then transferred onto Si substrates. Cellulose membrane supports were dissolved thoroughly using a multiple acetone baths cleaning process, leaving GO films ready for UPS measurements. Deposited GO thin films were also used for XPS and electrical measurements (SiO_2/Si substrates).

For the transmission electron microscopy and photocurrent map, a synthesized GO aqueous suspension was diluted further and drop-cast onto mesh grids and prepatterned SiO_2/Si substrates, respectively, to obtain isolated individual GO sheets. For the photocurrent map, the positions of the monolayer GO individual sheets with respect to the alignment marks were identified under the optical microscope and conventional electron-beam lithography was used to define electrodes on the sheets. The GO sheets were contacted by thermally evaporating Ti/Au (5/30 nm) followed by a lift-off process.

2.2 Real-time UPS measurements UPS was performed in an ultrahigh vacuum (UHV) chamber with a base pressure of $\sim 1 \times 10^{-8}$ Pa. Specimen were gradually heated *in situ* to ~850 in 50 °C increments. At every 50 °C step, the temperature was held constant for ~700 s while UPS was performed. A He-I resonance line ($h\nu = 21.22$ eV) was used as an excitation source. We used a pulsed heating method to remove artificial effects on the data from magnetic and electric fields induced by the electric current used for the Joule heating of the specimen (Fig. 1a). An Mo plate in contact with GO was used as a reference for obtaining Fermi level of the specimen. The specimen was negatively biased (−7 V) to allow efficient collection of secondary electrons near the vacuum level. The energy resolution of the measurement was ~0.10 eV with a pass energy of 10 eV.

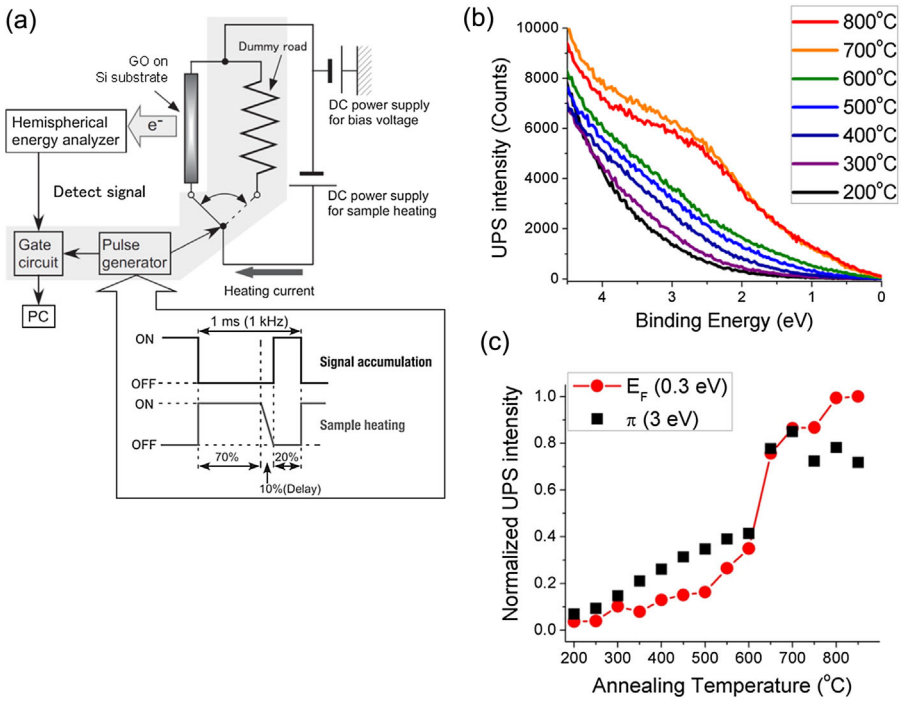

Figure 1 (a) Schematic of UPS measurement setup and the procedures used in this study. (b) UPS spectra as a function of annealing temperature for an energy range between E_F and 5 eV into the valence band (VB) of GO. The intensity is in counts and has not been processed. (c) UPS intensity evolution for carbon 2p π bonds and E_F. The intensity is normalized for demonstration purposes to the maximum of each of π bonds and E_F.

Only the spectra for annealing temperature of 200 °C and above were analyzed in this study due to the possible charging effect for <200 °C.

2.3 Other material characterization

2.3.1 *Ex situ* thermal annealing of GO All of the thermal annealing of GO except for UPS was performed *ex situ*. More specifically, GO films on a substrate were placed in a quartz tube furnace and heated to a targeted temperature in the presence of an inert gas (N_2) and held for 15 min.

2.3.2 X-ray photoelectron spectroscopy (XPS) XPS measurements were performed with a Thermo Scientific K-Alpha spectrometer. All spectra were taken using an Al Kα microfocused monochromatized source (1486.6 eV) with a resolution of 0.6 eV. The spot size was 400 μm and the operating pressure was 5×10^{-9} Pa. The GO thin films were measured on a Pt foil and Pt $4f_{7/2}$ was taken as a reference at 70.98 eV.

2.3.3 High-resolution transmission electron microscopy (HRTEM) HRTEM was performed using a JOEL JEM-2100F TEM/STEM with double spherical aberration (C_s) correctors (CEOS GmbH, Heidelberg, Germany) to attain high-contrast images with a point-to-point resolution of 1.4 Å. The lens aberrations were optimized by evaluating the Zemlin tableau of an amorphous carbon. The residual spherical aberration was almost zero ($C_s = -0.8 \pm 1.2$ μm with 95% certification). The acceleration voltage was set to 120 kV, which is the lowest voltage with effective C_s correctors in the system. The region of interest was focused upon and then recorded with a total exposure of less than 20 s (0.5 s exposure time for the image).

2.3.4 Electrical measurements The electrical conductivity of GO thin films was obtained from the sheet resistance measured using a standard Van der Pauw method. A Keithley 2400 sourcemeter was connected to four indium contacts soldered on each corner of the GO thin films. The film size used for the measurements was typically 15×15 mm^2 and the area of the indium contacts was kept to less than 1×1 mm^2. We have confirmed that the sheet resistance measured by the Van der Pauw method and the conventional two-probe method with Au contacts (length: 20 μm, width: 400 μm) results in similar values.

2.3.5 Scanning photocurrent microscopy (SPCM) A green diode-pumped solid-state laser ($\lambda = 532$ nm) was coupled through a confocal microscope via a 100× Olympus objective with a 0.9 numerical aperture to scan over the specimen to form a photocurrent map [32, 33]. The laser spot size was ~400 nm. The laser power was kept to less than 1 mW to prevent possible thermal reduction as well as damage to the GO/rGO devices. Synchronous detection was achieved via a SR-830 lock-in amplifier (Stanford Research

Systems) using the reference frequency input from the chopper (~370 Hz). The photocurrent signal was first amplified by a SR-570 current amplifier (Stanford Research Systems) and the AC component of the output voltage signal was used as a direct input to the lock-in amplifier. Both the amplitude R and the phase ϕ of the photocurrent were monitored. Correlated PL obtained for the same position of SPCM map was detected using an avalanche photodiode, allowing determination of the exact location of individual monolayer GO sheet device and the contact electrodes. 1 V was applied between the electrodes for the measurements performed in this study. A center region of the device was used for fixed-spot measurements.

3 Results and discussion

3.1 UPS and electrical conductivity Figure 1a shows a schematic of the UPS measurement setup and the procedures used in this study. The uniqueness of our method is the use of pulsed heating sequence to prevent the effects of magnetic and electric field on collected photoelectrons. The advantage is that data taken at different temperatures can be compared directly without generally required calibrations. Figure 1b shows the annealing temperature-dependent UPS spectra for the range from the Fermi level E_F to 5 eV into the VB, which provides information on DOS for carbon 2p π bonds (3 eV) and the Fermi level E_F (0 eV) of GO (see Experimental section for determination of E_F). The spectra for an annealing temperature of 200 °C and above are shown to exclude the charging effect. After a gradual increase for the π bonds and E_F up to ~600 °C, an unexpected drastic increase was observed between 600 and 650 °C for both cases. In order to gain further insights into the details of the evolution, the UPS intensity at 3 and 0.3 eV was plotted as a function of annealing temperatures (Fig. 1c) [34, 35]. 0.3 eV was used instead of 0 eV for E_F merely for its higher intensity with an identical evolution behavior. The results clearly show a drastic increase of DOS at the π bonds and E_F between 600 and 650 °C, which indicates a bandgap closure. After the drastic increase between 600 and 650 °C, the π bonds show a gradual decrease, while the E_F continues to increase at a reduced rate. One possible scenario for the observed trend is a formation of vacancy defects that are reported to occur around the temperature range [35]. Desorption of oxygen groups such as carbonyl and ether in the form of CO or CO_2 causes loss of carbon atoms in the basal plane of GO. These losses can lead to a slight decrease of the π bonds above 650 °C. On the other hand, formations of vacancy defects increases the number of dangling bonds (i.e., edge states) in the material system, and hence could lead to the observed gradual increase of DOS at E_F [36].

The observed drastic increase of DOS for the π bonds and E_F between 600 and 650 °C is unexpected because the temperature range is quite different from what can be expected from the well-established knowledge of sharp restoration in electrical conductivity. Figure 2a shows a comparison of evolution between electrical conductivity and UPS intensity as a function of annealing temperature. The difference of annealing temperature at which the sharp rise is observed in electrical conductivity and the DOS at E_F is clearly demonstrated (purple arrow). One example where the difference would play an important role is upon a design of GO-based optoelectronics. For an optoelectronic device such as a photodetector, one must consider a balance between electrical conductivity and possession of a bandgap. Specifically, a higher electrical conductivity leads to a better device performance but a material should not be metallic as it will lose the photoresponse. Therefore, in a material like GO that undergoes semiconductor to semimetal transitions upon thermal annealing, it is crucial to identify the annealing temperature that leads to the material's maximum electrical conductivity but still remain a bandgap. Figure 2b shows an inverse of normalized UPS intensity at E_F and electrical conductivity as a function of annealing temperature. As the UPS intensity at E_F can be used to determine the annealing temperature that a bandgap closes (transition to metallic/semimetal), its inverse could be used as an indication of the materials photoresponse. To be

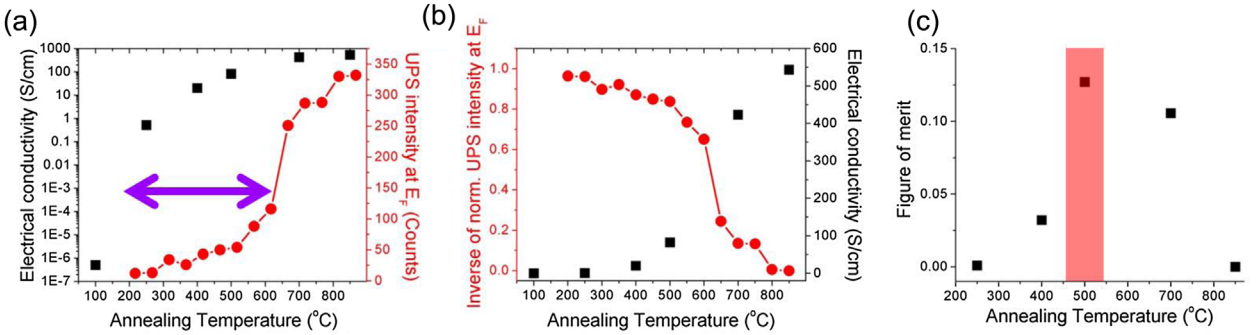

Figure 2 (a) Comparison between the evolution of electrical conductivity (black) and UPS intensity at E_F (red) as a function of annealing temperature. Electrical conductivity is shown in a log scale in S cm^{-1}, and the UPS intensity is in a linear scale in counts. (b) Comparison between the inverse of UPS intensity at E_F (red) and electrical conductivity (black) as a function of annealing temperature. The UPS intensity is normalized to its maximum value, and the conductivity is in S cm^{-1}. Both of them are plotted in a linear scale. (c) Multiples of two parameters shown in (b). The pink bar serves as a guide for the eye.

more specific, an inverse of UPS intensity drops drastically between 600 and 650 °C for GO, indicating the loss of its optical activity in this annealing temperature range. Based on the above-mentioned idea, one can consider a figure of merit as shown in Fig. 2c to obtain a quantitative temperature range for the optimal GO-based optoelectronic devices. The figure plots the multiple of two parameters shown in Fig. 2b; the electrical conductivity and inverse of UPS intensity at E_F. The result suggests that optoelectronic properties can be maximized after annealing the GO at around ~500 °C.

3.2 XPS and HRTEM XPS and HRTEM were performed to gain insights into the possible origin for the drastic increase of DOS at the π bonds and E_F. The simplest scenario for the observed increase is due to the increase of sp^2 carbon content around that annealing temperature range. If this were the case, then it could well explain both the increase of DOS at the π bonds and E_F. However, based on our XPS analysis as shown in Fig. 3a, there is no drastic increase of sp^2 carbon in the temperature range between 600 and 650 °C (see Supporting Information for details, online at: www.pss-a.com). Furthermore, the gradual increase of sp^2 carbon in the temperature range is consistent with a gradual decrease of O1s. Therefore, the XPS results demand for an alternative explanation for the observed DOS increase.

Figure 3b and c show the HRTEM image of as-synthesized GO and after annealing at 200 °C, respectively. Due to the high density of oxygen functional groups that are inhomogeneously attached to the graphene basal plane, no crystalline features are observed in (b). This trend is consistent with the literature reporting sp^2 carbon clusters/graphene nanoislands in the small domain size of <1 nm [37]. Density variations of graphene nanoislands between the literature and this study are most likely due to minor variations in the synthesis procedures. The observed amorphous nature of as-synthesized GO is the most probable origin of its bandgap. Based on the well-studied case of amorphous carbon (a-C), a mixture of sp^2 and sp^3 carbon with sp^2 fraction of ~40 at.% (similar to the as-synthesized GO case) is sufficient to explain the gap of a few eV [38]. When GO is annealed at 200 °C, graphene nanoislands of an average lateral size of ~2 nm are clearly observed, in contrast to the as-synthesized case (shown in red circles) (Fig. 3c). Moreover, a closer look at the images suggests possible percolation starting between graphene nanoislands in the close proximity via sp^2 carbon links or chains (shown in blue circles). Percolation of graphene nanoislands that is already occurring at 200 °C is expected to proceed further as annealing temperature increases (as some literature has shown up to ~550 °C) [37].

A driving force for the percolation is most likely a combination of the increased diffusion rate of oxygen functional groups at elevated temperatures and their energy-favorable clustering. As for diffusion rates of oxygen groups, the Arrhenius law $G = G_0 \exp(-E/kT)$, where G is the rate of diffusion, G_0 is the rate constant, and E is the migration barrier, indicates that they increase by orders of magnitude at 600 °C compared to the room-temperature case. For example, a diffusion rate of hydroxyl group, which is a groups known to remain at 600 °C, increased by as much as five orders of magnitude compared to that at room temperature when using the reported diffusion barrier of 0.53 eV [36]. In addition, a tendency of oxygen functional groups in GO to form clusters based on chemical kinetics was recently demonstrated by Kumar et al. [39]. This is supported by our HRTEM results on GO, which showed formation of graphene nanoislands (i.e., oxygen clusters) after annealing at 200 °C (Fig. 3c). Although more detailed analysis will be required to conclude on the origin of the drastic increase of DOS at E_F, our basic material characterization points toward enlargement of the effective graphene-islands via percolation as a possibility.

3.3 SPCM In order to demonstrate that optimal annealing conditions for GO optoelectronic devices can be determined based on a combination of DOS at E_F

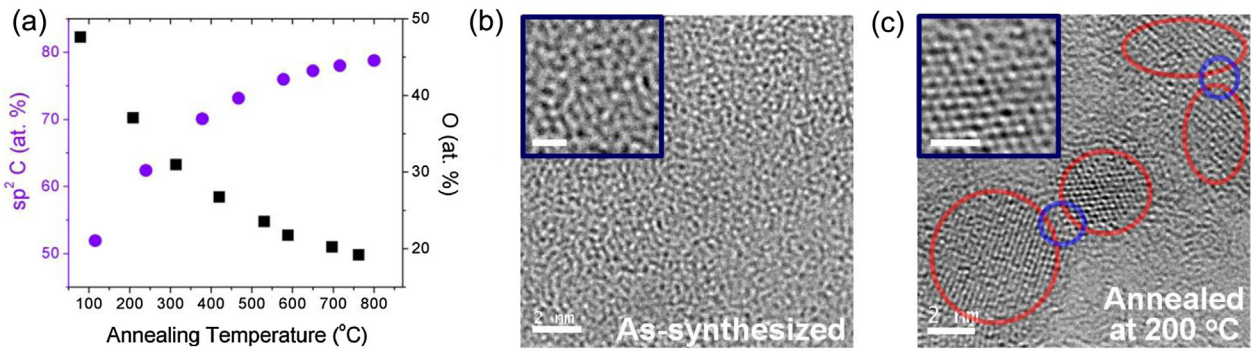

Figure 3 (a) sp^2 carbon (purple) and O1s (black) contents obtained by XPS as a function of annealing temperature. (b) HRTEM of as-synthesized GO. (c) HRTEM image of GO thermally annealed at 200 °C. The red circles indicate regions of sp^2 graphene nanoisland clusters, and blue circles indicate regions of sp^2 graphene percolation chains. Scale bars for (b) and (c) are 2 nm, and they are 1 nm for insets.

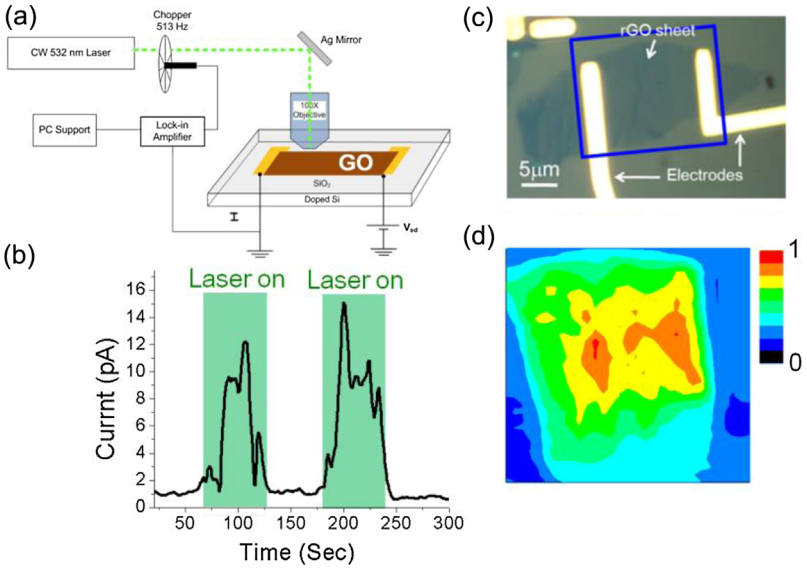

Figure 4 (a) Schematic of SPCM setup. (b) Photocurrent–time characteristics of GO individual sheet device shown in (c). Fixed-spot laser illumination ($\lambda = 532$ nm) was turned on and off periodically as shown with light green bars. (c) Optical microscope image of a device used to obtain (b) and (d). The blue rectangular region indicates the region of (d) SPCM map. Scale bar is 5 μm. (d) SPCM map of individual rGO sheet device annealed at ~500 °C. The size of the map is $\sim 10 \times 10\ \mu m^2$. The photocurrent is normalized to its maximum value, with red indicating the maximum intensity and black indicating the minimum.

and the electrical conductivity, the photocurrent of an individual GO sheet was obtained. Specifically, two forms of data were obtained using scanned photocurrent microscopy (SPCM) (see Experimental section for details); a fixed-spot current–time characteristic, and a spatial map [32, 33]. We used an annealing temperature of ~500 °C based on the figure of merit shown in Fig. 2c. The results indeed proved that high optoelectronic performance can be achieved in devices that were annealed in the temperature range. While as-synthesized GO did not exhibit any photocurrent above the measurement noise level (~1 pA), the device annealed at ~500 °C exhibits an order of magnitude enhancement in photocurrent when laser illumination was on the device (9–15 pA, Fig. 4b). Moreover, the map showed uniform and enhanced photocurrent over the entire rGO sheet with a channel length of as large as >10 μm (Fig. 4c and d).

4 Conclusions In summary, VB electronic structure evolutions of GO upon thermal reduction are characterized by real-time UPS. DOS around the Fermi level showed a sharp increase at annealing temperatures between 600 and 650 °C, indicating a bandgap closure. Correlation between the evolution of DOS at E_F and chemical/structural properties indicated that a percolation of sp^2 carbon as a possible origin. In addition, a combination of UPS and electrical measurements results suggested that annealing GO at a temperature of ~500 °C would lead to material properties suitable for optoelectronics. This was successfully demonstrated by a uniform and an order of magnitude enhancement in photocurrent map for an individual GO sheet reduced in the same temperature range. Our results provide experimental evidence that demonstrates the importance of studying the electronic structures in accordance with other material characterization techniques in achieving optimized device performances, such as for graphene-based optoelectronic devices.

Supporting Information Additional supporting information may be found in the online version of this article at the publisher's web-site.

Acknowledgments The authors acknowledge T. Kaga and S. Takabayashi of Tohoku University, Japan, and E. Cheng and D. Voiry of Rutgers University for the experimental support. The authors also acknowledge Asbury Carbon, NJ for generously supplying the starting graphite powders as a part of their U.S. national laboratory supporting program. H. Y. and M. C. acknowledge Donald H. Jacobs' Chair funding from Rutgers University. H. Y. acknowledges the Laboratory Directed Research and Development (LDRD) Director's Postdoctoral Fellowship of LANL, and the Japanese Society for the Promotion of Science (JSPS) Postdoctoral Fellowship for Research Abroad for financial support. This work was performed under the Cooperative Research Program of the "Network Joint Research Center for Materials and Devices" by the Ministry of Education, Culture, Sports, Science and Technology (MEXT), Japan. The XPS measurements using synchrotron radiation were performed at BL23SU in SPring-8 under the "Nano-net Project" of the Japan Synchrotron Research Institute (JASRI) and Japan Atomic Energy Agency (JAEA) (proposal Nos. 2010A3874, 2010B3879, and 2014B3874). The research was also supported by the LDRD Program and performed, in part, at the Center for Integrated Nanotechnologies, an Office of Science User Facility operated for the US Department of Energy (DOE) Office of Science. Los Alamos National Laboratory, an affirmative action equal opportunity employer, is operated by Los Alamos National Security, LLC, for the National Nuclear Security Administration of the US Department of Energy under contract DE-AC52-06NA25396.

References

[1] A. K. Geim and K. S. Novoselov, Nature Mater. **6**, 183 (2007).
[2] K. S. Novoselov, V. I. Falko, L. Colombo, P. R. Gellert, M. G. Schwab, and K. Kim, Nature **490**, 192 (2012).
[3] A. S. Mayorov, R. V. Gorbachev, S. V. Morozov, L. Britnell, R. Jalil, L. A. Ponomarenko, P. Blake, K. S. Novoselov,

K. Watanabe, T. Taniguchi, and A. K. Geim, Nano Lett. **11**, 2396 (2011).
[4] R. R. Nair, P. Blake, A. N. Grigorenko, K. S. Novoselov, T. J. Booth, T. Stauber, N. M. R. Peres, and A. K. Geim, Science **320**, 1308 (2008).
[5] C. Lee, X. D. Wei, J. W. Kysar, and J. Hone, Science **321**, 385 (2008).
[6] T. Ohta, A. Bostwick, T. Seyller, K. Horn, and E. Rotenberg, Science **313**, 951 (2006).
[7] X. Li, X. Wang, L. Zhang, S. Lee, and H. Dai, Science **319**, 1229 (2008).
[8] J. Cai, P. Ruffieux, R. Jaafar, M. Bieri, T. Braun, S. Blankenburg, M. Muoth, A. P. Seitsonen, M. Saleh, X. Feng, K. Mullen, and R. Fasel, Nature **466**, 470 (2010).
[9] D. C. Elias, R. R. Nair, T. M. G. Mohiuddin, S. V. Morozov, P. Blake, M. P. Halsall, A. C. Ferrari, D. W. Boukhvalov, M. I. Katsnelson, A. K. Geim, and K. S. Novoselov, Science **323**, 610 (2009).
[10] J. T. Robinson, J. S. Burgess, C. E. Junkermeier, S. C. Badescu, T. L. Reinecke, F. K. Perkins, M. K. Zalalutdniov, J. W. Baldwin, J. C. Culbertson, P. E. Sheehan, and E. S. Snow, Nano Lett. **10**, 3001 (2010).
[11] R. R. Nair, W. Ren, R. Jalil, I. Riaz, V. G. Kravets, L. Britnell, P. Blake, F. Schedin, A. S. Mayorov, S. Yuan, M. I. Katsnelson, H.-M. Cheng, W. Strupinski, L. G. Bulusheva, A. V. Okotrub, I. V. Grigorieva, A. N. Grigorenko, K. S. Novoselov, and A. K. Geim, Small **6**, 2877 (2010).
[12] R. Balog, B. Jorgensen, L. Nilsson, M. Andersen, E. Rienks, M. Bianchi, M. Fanetti, E. Laegsgaard, A. Baraldi, S. Lizzit, Z. Sljivancanin, F. Besenbacher, B. Hammer, T. G. Pedersen, P. Hofmann, and L. Hornekaer, Nature Mater. **9**, 315 (2010).
[13] E. Stratakis, K. Savva, D. Konios, C. Petridis, and E. Kymakis, Nanoscale **6**, 6925 (2014).
[14] M. M. Stylianakis, M. Sygletou, K. Savva, G. Kakavelakis, E. Kymakis, and E. Stratakis, Adv. Opt. Mater. **3**, 658 (2015).
[15] M. Z. Hossain, J. E. Johns, K. H. Bevan, H. J. Karmel, Y. T. Liang, S. Yoshimoto, K. Mukai, T. Koitaya, J. Yoshinobu, M. Kawai, A. M. Lear, L. L. Kesmodel, S. L. Tait, and M. C. Hersam, Nature Chem. **4**, 305 (2012).
[16] S. Stankovich, D. A. Dikin, R. D. Piner, K. A. Kohlhaas, A. Kleinhammes, Y. Jia, Y. Wu, S. T. Nguyen, and R. S. Ruoff, Carbon **45**, 1558 (2007).
[17] G. Eda, G. Fanchini, and M. Chhowalla, Nature Nanotechnol. **3**, 270 (2008).
[18] C.-N. Yeh, K. Raidongia, J. Shao, Q.-H. Yang, and J. Huang, Nature Chem. **7**, 166 (2015).
[19] C. Mattevi, G. Eda, S. Agnoli, S. Miller, K. A. Mkhoyan, O. Celik, D. Mastrogiovanni, G. Granozzi, E. Garfunkel, and M. Chhowalla, Adv. Funct. Mater. **19**, 2577 (2009).
[20] X. Gao, J. Jang, and S. Nagase, J. Phys. Chem. C **114**, 832 (2010).
[21] A. Mathkar, D. Tozier, P. Cox, P. Ong, C. Galande, K. Balakrishnan, A. Leela Mohana Reddy, and P. M. Ajayan, J. Phys. Chem. Lett **3**, 986 (2012).
[22] H. F. Liang, C. T. G. Smith, C. A. Mills, and S. R. P. Silva, J. Mater. Chem. C **3**, 12484 (2015).
[23] P. Sun, Y. Wang, H. Liu, K. Wang, D. Wu, Z. Xu, and H. Zhu, PLOS ONE **9**, e111908 (2014).
[24] M. Kang, D. H. Lee, J. Yang, Y. M. Kang, and H. Jung, RSC Adv. **5**, 104502 (2015).
[25] E. Kymakis, K. Savva, M. M. Stylianakis, C. Fotakis, and E. Stratakis, Adv. Funct. Mater. **23**, 2742 (2013).
[26] C. Gómez-Navarro, R. T. Weitz, A. M. Bittner, M. Scolari, A. Mews, M. Burghard, and K. Kern, Nano Lett. **7**, 3499 (2007).
[27] G. Eda, C. Mattevi, H. Yamaguchi, H. Kim, and M. Chhowalla, J. Phys. Chem. C **113**, 15768 (2009).
[28] L. J. Cote, R. Cruz-Silva, and J. Huang, J. Am. Chem. Soc. **131**, 11027 (2009).
[29] Y. K. Jo, I. Y. Kim, S.-j. Kim, S. I. Shin, A. Go, Y. Lee, and S.-J. Hwang, RSC Adv. **5**, 19259 (2015).
[30] A. Ganguly, S. Sharma, P. Papakonstantinou, and J. Hamilton, J. Phys. Chem. C **115**, 17009 (2011).
[31] M. Hirata, T. Gotou, S. Horiuchi, M. Fujiwara, and M. Ohba, Carbon **42**, 2929 (2004).
[32] A. D. Mohite, D. E. Perea, S. Singh, S. A. Dayeh, I. H. Campbell, S. T. Picraux, and H. Htoon, Nano Lett. **12**, 1965 (2012).
[33] H. Yamaguchi, J.-C. Blancon, R. Kappera, S. Lei, S. Najmaei, B. D. Mangum, G. Gupta, P. M. Ajayan, J. Lou, M. Chhowalla, J. J. Crochet, and A. D. Mohite, ACS Nano **9**, 840 (2014).
[34] R. Larciprete, P. Lacovig, S. Gardonio, A. Baraldi, and S. Lizzit, J. Phys. Chem. C **116**, 9900 (2012).
[35] A. Bagri, C. Mattevi, M. Acik, Y. J. Chabal, M. Chhowalla, and V. B. Shenoy, Nature Chem. **2**, 581 (2010).
[36] T. O. Wehling, M. I. Katsnelson, and A. I. Lichtenstein, Phys. Rev. B **80**, 085428 (2009).
[37] K. Erickson, R. Erni, Z. Lee, N. Alem, W. Gannett, and A. Zettl, Adv. Mater. **22**, 4467 (2010).
[38] J. Robertson, Mater. Sci. Eng. R, Rep. **37**, 129 (2002).
[39] P. V. Kumar, N. M. Bardhan, S. Tongay, J. Wu, A. M. Belcher, and J. C. Grossman, Nature Chem. **6**, 151 (2014).